Research and Development of Neutron Detection System using Scintillator and Digital-Signal Processing

Kouji SHINOHARA, Keiichi ISHII[1)], Kentaro OCHIAI, Mamoru BABA[2)], Mamiko SASAO[3)] and Sumio KITAJIMA[1)]

Japan Atomic Energy Agency, Naka, Ibaraki 311-0193, Japan
[1)]*Department of Quantum Science and Energy Engineering, Tohoku University, Sendai, Miyagi 980-8579, Japan*
[2)]*Cyclotron and Radioisotope Center, Tohoku University, Sendai, Miyagi 980-8578, Japan*
[3)]*Organization for Research Initiatives and Development, Doshisha University, Kyotanabe, Kyoto 610-0321, Japan*

(Received 8 July 2013 / Accepted 26 August 2013)

A collimated neutron flux array system in JT-60U successfully upgraded performance of higher counting rate and the capability to detect 14 MeV neutrons as well by using a fast digitizer in 2006. Additionally, detailed analysis of the recorded waveform on JT-60U and FNS has provided us new findings. In this paper, firstly, characteristics of pulse shapes and neutron-gamma discrimination parameters investigated by the detailed analysis of digitized waveform data are described. Next, new data analysis procedure for neutron-gamma discrimination based on the characteristics is proposed. In the new procedure, an appropriate projection surface, on which we can define the discrimination boundary, has been introduced in three-dimensional discrimination parameter space. The problem of "pulse height variation", which occurs when a counting rate is high in high performance plasma, and its countermeasures are also presented. The system using the countermeasure of a booster method successfully has avoided the problem in the high neutron flux condition of $\sim 2 \times 10^5$ counts/s on FNS.

Keywords: neutron measurement, neutron-gamma discrimination, scintillator, fast digitizer, JT-60U, FNS

DOI: 10.1585/pfr.8.1402144

1. Introduction

Plasma will be heated by alpha particles, which are one of fusion products and fast ions, in fusion reactors. The fast ions also play an important role in current drive. The research relating to the fast ion behavior is an important topic in ITER and present-day devices because plasma heating and current drive are key topics for high performance plasma development. In investigating the fast ion behavior, it is preferable to measure a phase space distribution with high time- and space-resolution. However, such a measurement has not been realized yet by one diagnostics. The several diagnostics, such as line-integrated neutron emission neutron diagnostics [1–4], fast ion Dalpha (FIDA) diagnostics [5], fast ion loss detector (FILD) diagnostics [6, 7], and fast neutral flux diagnostics [8–10], have been used to pick up the aspects of the phase space distribution.

Since the neutron is emitted effectively by nuclear reaction involving fast ions, the measurement of line-integrated neutron emission signals brings us the information on the fast ion profile. Thus, on many present-day devices, collimated neutron detection array system, which is also called as a neutron camera, is installed to measure a line-integrated neutron emission. It is considered that neutron camera will be installed on ITER, too. In JT-60U, d-D neutron detectors equipped with analog neutron-gamma (n-γ) pulse shape discrimination circuits [4] was installed in 2000. Here, d-D neutrons are emitted with the energy of 2.5 MeV by deuterium-deuterium reaction. This system has contributed to the research on the fast ion confinement during plasma instabilities [11–13] and beam-driven current drive studies [14].

The system had, however, defects that the count rate of the n-γ discrimination circuit was limited below $\sim 1 \times 10^5$ counts/s and that the system can detect only d-D neutrons. To overcome the defects, a system using a fast flash analog-to-digital converter (flash ADC) was developed [15, 16]. In this system, output pulses from an anode of a photomultiplier tube (ELT 9266B type manufactured by Electron Tube Ltd.) for the detector are recorded as a continuous waveform using a fast flash ADC with 200 MS/s permitting pulse pile-up, and the recorded data is analyzed with software off-line. The n-γ discrimination was a post-process. The photomultiplier and its base were of fast response and high-peak current. This system successfully achieved the counting rate higher than 1×10^5 counts/s (cps) and also enabled the observation of d-T neutrons with the energy of 14 MeV from deuterium-tritium reaction [17–19].

Since the entire waveform of the pulses from a detector was recorded, this method revealed many detailed

author's e-mail: shinohara.koji@jaea.go.jp

features in neutron detection using an organic scintillator. This paper presents new features obtained by using the system. Section 2 describes the neutron detection system using the flash ADC briefly at first. Then, in Sec. 3, the characteristics of the pulse shape and discrimination parameters observed in experiments are described in detail, and we propose a new data analysis procedure based on this newly obtained knowledge. We have introduced the analysis procedure to find an appropriate projection surface, on which we can define the discrimination boundary, in the three-dimensional space of the discrimination parameters. Section 4 treats an issue referred to as a "pulse height variation" which is the phenomenon that the pulse height of large signal varies during a discharge with a count rate. The observed characteristics of the "pulse height variation" in experiments in JT-60U tokamak and a 14 MeV neutron beam in the Fusion Neutronics Source (FNS) at JAEA are described. In Sec. 4, we also describe the countermeasure to overcome this "pulse height variation" issue. At the end, this work is summarized.

2. Neutron Detection System using the Flash ADC and Characteristics of Pulse Shape

Figure 1 shows the block diagram of the collimated neutron flux array system using the flash ADC installed at the JT-60 torus hall. The sight lines of the multi-chords are also depicted. Detectors were organic stilbene crystals. The size of the stilbene crystal is 1" in length ×1" in diameter. The flash ADCs and a computer for the ADC control are installed in a basement room on the downstairs of the torus hall to guard from the strong neutron radiation. The hardwired cable between detectors and the ADCs is about 20 m long for oblique chords and about 30 m long for a vertical chord [15–17]. The sampling rate of the ADCs was 200 M samples/s, which was chosen as a compromise between the pulse shape discrimination quality, and the time period covered by the system due to the limitation of the memory in ADC. Namely, data can be captured for 2.7 sec when the sampling rate is 200 M samples/s, and on the other hand, data can be captured only for 0.27 sec when the rate is 2 G samples/s for a better capturing of the pulse shape, while research on plasma physics requires the acquisition time longer than 1 sec because the time scale of the slowing-down time of the fast ions reaches > 1 sec. This is the background of the selection of the sampling rate of 200 M samples/s.

The n-γ discrimination was carried out using the so-called "charge comparison method" in which each pulse was integrated for two different time intervals, "fast" and "slow", and the ratio of two integrated charges is compared [17]. In the digital process, the surface area of the pulse shape in a time interval corresponds to "charges". Namely, we define discrimination parameters of Q_{fast},

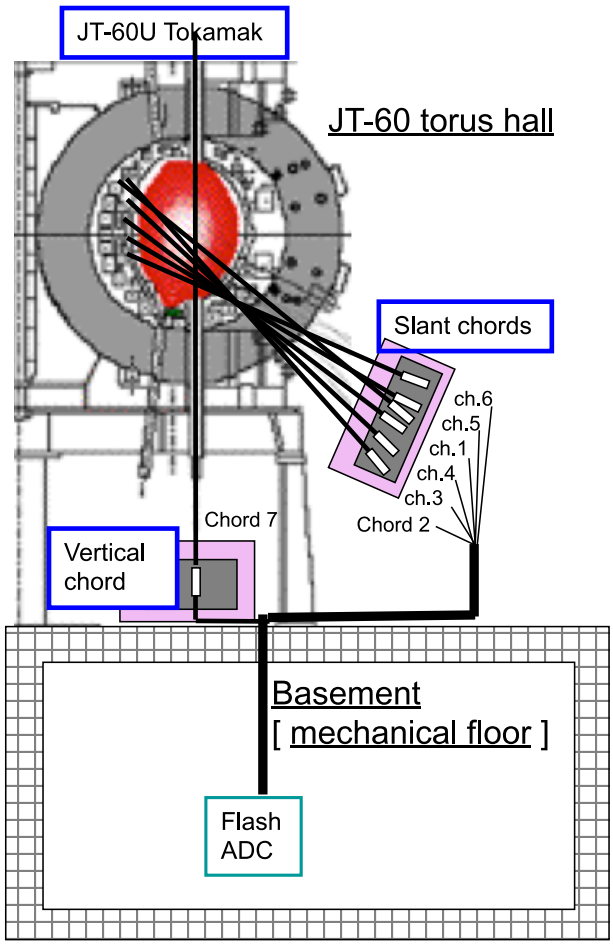

Fig. 1 Schematic view of the collimated neutron flux array system using the flash ADC on JT-60U.

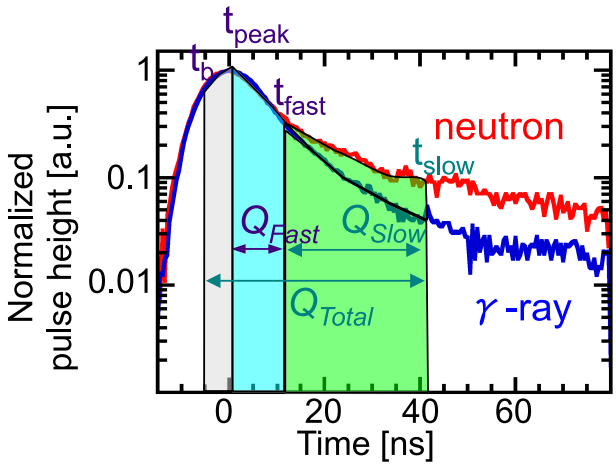

Fig. 2 Normalized waveforms for pulses induced by a neutron and a γ-ray. A curve in red shows the waveform of a pulse by a neutron, and a curve in blue shows that by a γ-ray. The definition of t_{b}, t_{peak}, t_{fast}, t_{slow}, Q_{fast}, Q_{slow} and Q_{total} is also illustrated.

Q_{slow} and Q_{total} as the surface area in t_{peak} through t_{fast}, in t_{fast} through t_{slow}, and in t_{b} through t_{slow}, respectively, as shown in Fig. 2. The n-γ discrimination uses the charac-

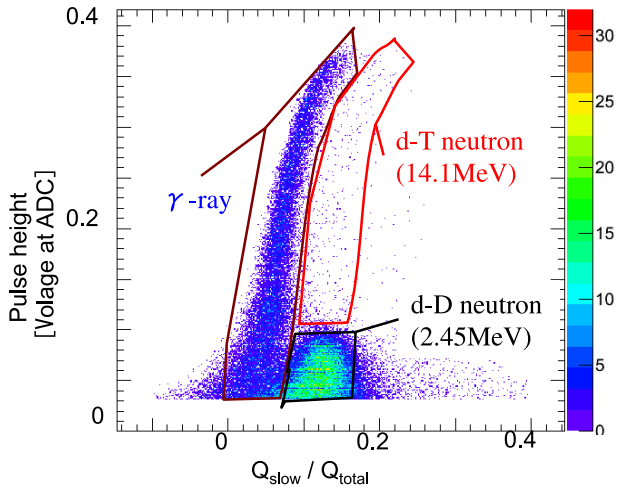

Fig. 3 Pulse density plot on height versus Q_{slow}/Q_{total} for data obtained on JT-60U. Each dot corresponds to each pulse. The color indicates the density of dots or pulses in a grid cell. The number of cells is 400 in the vertical direction, and 400 in the horizontal direction. Note: due to the effect of the bipolar noise of ~1 mV, the signal can be negative in the slave of a low-pulse-height pulse at a time. That is the reason why the $Q_{slow}/Q_{total} < 0$ for the gamma-ray pulses with low pulse height.

teristics that the time scale of a slow component or a long tail of the pulse originated from a neutron is longer than that originated from a γ-ray. Due to the characteristics, the value of Q_{slow}/Q_{total} for a neutron is larger than that for a γ-ray.

In Fig. 3, a two-dimensional plot for the pulse height versus Q_{slow}/Q_{total} is shown. Each dot corresponds to each pulse. The color indicates the density of the dots in a grid cell on the plot, where the number of cells is 400 in the direction of the pulse height and 400 in the direction of Q_{slow}/Q_{total}. A group of dots with relatively smaller value of Q_{slow}/Q_{total} at a given pulse height consists of the pulses from γ-rays. The dots next to the group are dots for neutrons. We can identify a structure of neutrons events in these dots. Namely, there are a dense area and a sparse area. The dense area lies in the low pulse height region. This structure comes from the difference of the number of two kinds of neutrons, namely their energy difference in deuterium plasmas. In the deuterium plasma, the following nuclear reactions produce two kinds of neutrons,

$$\mathrm{D + D \rightarrow {}^3He + n\ (d\text{-}D\ neutron\ with\ 2.5\,MeV)},$$
$$\mathrm{D + D \rightarrow T + p;\ D + T \rightarrow \alpha + n}$$
$$\mathrm{(d\text{-}T\ neutron\ with\ 14.1\,MeV)}.$$

As shown in the second line, d-T neutrons are produced by a cascade of two reactions. The production of d-T neutrons is less than that of d-D neutrons due to small triton density. The higher energy neutron induces a pulse with a higher pulse height. Thus, the d-T and d-D neutrons can be discriminated by using the difference of the pulse height.

Therefore, firstly, pulses due to neutrons and γ-rays can be discriminated by the length of the long tail, and secondly, pulses due to d-T and d-D neutrons can be discriminated by the pulse height. These are the overview of the discrimination procedure. However, it was found that the procedure is not always simple, after understanding the characteristics of the data recorded by this fast digitizer in detail. Hereafter, we will describe the characteristics and the analysis procedure we have developed in light of the characteristics.

3. Characteristics of Pulse Shape and Improved n-γ Discrimination Procedure

As mentioned above, the n-γ discrimination is based on the fact that the decay time differs between neutrons and γ-rays [18]. The difference comes from the scintillation mechanism. The scintillation for neutrons is a result of interaction with neutron-induced recoil protons, and that for γ-rays is that with electrons produced by the Compton scattering, photoelectric effect and pair-production of γ-rays. The decay shape consists of both a prompt component and a slow component or a long tail as can be seen in Fig. 2. The prompt component is associated with a single scintillation process due to the resonance transition from the first excited singlet state to the ground singlet state, and independent of the particles, which induce the excitation [18]. The difference appears mainly in the slow component, which is related to the intercombination transition from the triplet state to the ground singlet state. The excitation to the triplet state increases with increasing linear energy transfer. The slow component is larger for neutrons since the linear energy transfer is higher for protons than for electrons [18]. Thus, it is important to determine the optimum t_{fast}, at which the slow component becomes dominant in order to achieve the best quality of the discrimination.

Since we have digitized waveforms directly in our method, we can analyze the pulse shape in detail. The reasonable fitting makes it easier to define the characteristic time of t_{fast}. It is considered that the shape of the prompt component of the measured curve can be obtained by a convolution of the response function and the true decay curve. Here, we assume that the response function is Gaussian in shape, mainly due to the response of PMT, and that the true decay curve is exponential at the initial evolution since the prompt component is considered to be a single scintillation as mentioned above. Thus, the shape of the prompt component is assumed by

$$p(t) \propto \int_0^\infty \exp\left\{-\left(\frac{t-s}{b}\right)^2\right\} \cdot \exp\left\{-\frac{s}{d}\right\} ds$$
$$\propto \exp\left\{-\frac{t}{d}\right\}\left[1 + \mathrm{erf}\left(\frac{t}{b} - \frac{b}{2d}\right)\right],$$

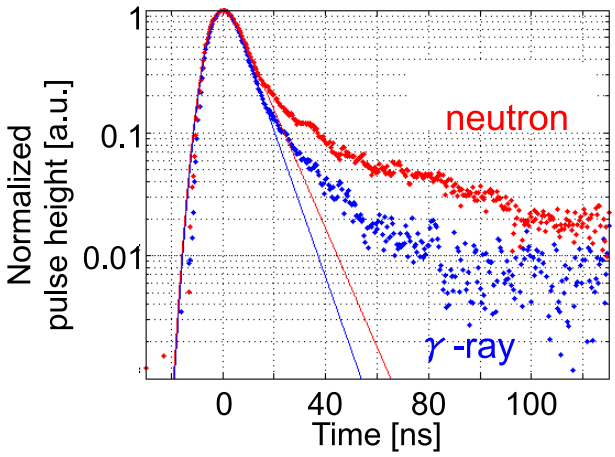

Fig. 4 Normalized waveforms of pulses with the modeled initial shapes. Each waveform is averaged one with eleven pulses that have similar pulse heights. Curves in red correspond to neutron signals, and curves in blue correspond to γ-ray signals.

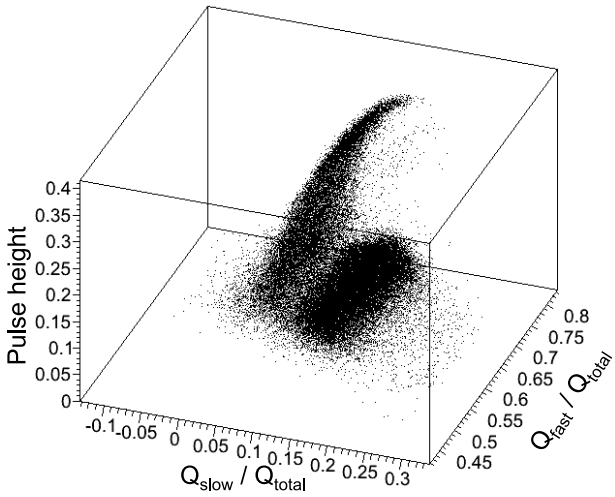

Fig. 5 Three-dimensional plot for parameters: Pulse height versus $Q_{\rm fast}/Q_{\rm total}$ versus $Q_{\rm slow}/Q_{\rm total}$. To highlight the issue, data with an apparent lower sampling rate of 200 M samples/s were artificially created from the data of 2 G samples/s.

where b is a decay parameter for the Gaussian, d is that for the exponential decay, and erf(x) is the error function. The calculated shape is plot in Fig. 4. We can see that this assumption is reasonable and that the fitted curve gives us a clear guide to define the characteristic time of $t_{\rm fast}$., where the slow component starts to be dominant.

We defined $Q_{\rm fast}$, $Q_{\rm slow}$ and $Q_{\rm total}$ as discrimination parameters. These parameters are equivalent to those used in "the charge comparison method" in an analog analysis. To know how to handle these parameters in the discrimination, we drew the 3 dimensional (3D) plot in terms of the pulse height, $Q_{\rm fast}/Q_{\rm total}$, and $Q_{\rm slow}/Q_{\rm total}$ in Fig. 5. We can observe the broad distribution of points and we can recognize that a single 2D plot, which is equivalent to a conventional analog analysis, was not always the best projection. Namely, there is a possibility that the γ-ray dots can hide "behind" the neutron dots when we use only the plot as in Fig. 3. Figure 6 (a) is the projection of Fig. 5 on $Q_{\rm fast}/Q_{\rm total} - Q_{\rm slow}/Q_{\rm total}$ plane. The spread of the dots can be seen in the direction of an arrow. The spread can deteriorate the discrimination when we use only a 2D plot as shown in Fig. 3. It was found this spread is mainly caused by the fact that the pulse peak is not always detected correctly. One reason of the misdetection is the sparseness of sampling points in pulse digitizing. Actually, data used in Fig. 6 (a) originated from the data used in Figs. 6 (b) and (c), which was recorded with a sampling rate of 2 G samples/s. In Figs. 6 (b) and (c), the data was analyzed using the data just as it is, while, in Fig. 6 (a), data are artificially created from the data of Fig. 6 (b) so that an apparent lower sampling rate was 200 M samples/s. Actually, the dispersion of signal is about twice larger for the data of 200 M samples/s than that for the data of 2 G samples/s when we compare between Figs. 6 (a) and (b), or Fig. 5 and Fig. 6 (c). We also found another reason of the misdetection of the peak. The reason is a noise in a signal. Even in the high sampling rate, we cannot avoid the effect of the noise, which has a time scale much shorter than that of the signal and amplitude higher than a few percent of the pulse amplitude.

On the basis of these observations, we propose the following discrimination procedure:

1) Coarsely we choose the time point of $t_{\rm fast}$. The time point should be chosen as the time when the long tail starts. We can choose the time point by assuming that the pulse shape has approximately line symmetry against peak time before $t = t_{\rm fast}$. Then, we calculate $Q_{\rm fast}$ and $Q_{\rm slow}$ as $t_{\rm slow} = 2 \times t_{\rm fast}$.
2) We draw a plot of pulse height versus $Q_{\rm slow}/Q_{\rm total}$ (e.g. Fig. 3). Then, we pick up pulses that are obviously regarded to be neutrons or γ-ray signals for the evaluation of the time points.
3) We reevaluate the time points of $t_{\rm fast}$ and $t_{\rm slow}$ by comparison of the pulse shapes for pulses obtained in the above procedure 2). (e.g. Fig. 4.)
4) A plot of $Q_{\rm fast}/Q_{\rm total}$ versus $Q_{\rm slow}/Q_{\rm total}$ is drawn using the reevaluated $t_{\rm fast}$ and $t_{\rm slow}$. Then, a line to separate neutron and gamma signals is determined as shown in Fig. 7 (a). The line is determined by the method using liner discriminant function described in Ref. [20]. This line is a surface in the 3D space of height, $Q_{\rm fast}/Q_{\rm total}$ and $Q_{\rm slow}/Q_{\rm total}$. We name the surface "$S_1$".
5) A plot of height versus $Q_{\rm fast}/Q_{\rm total}$ versus $Q_{\rm slow}/Q_{\rm total}$ was projected against the surface, named S_2, which is perpendicular to both the surface S_1 and the surface with the zero height. The projection on S_2 is shown in Fig. 7 (b).

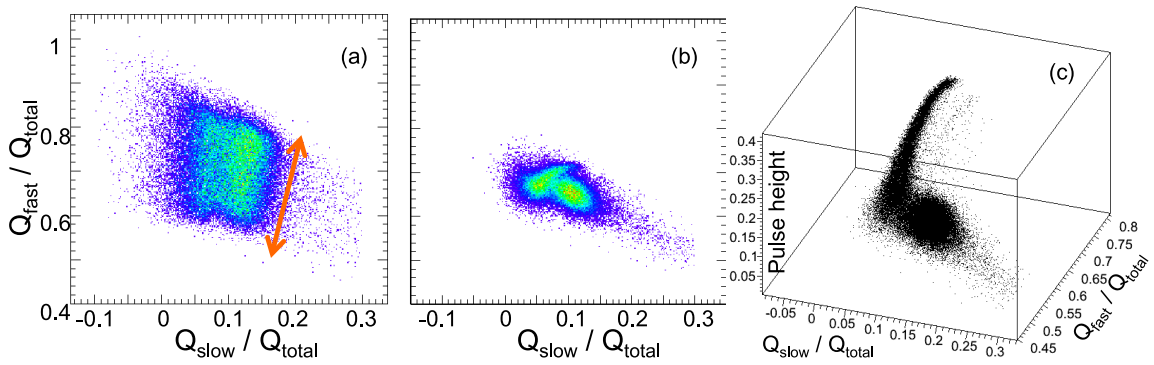

Fig. 6 (a) Pulse density plot on $Q_{\rm fast}/Q_{\rm total}$ versus $Q_{\rm slow}/Q_{\rm total}$ plane for the artificial data of 200 MS/s in Fig. 5. (b) Plot on $Q_{\rm fast}/Q_{\rm total}$ versus $Q_{\rm slow}/Q_{\rm total}$ plane for the original data of 2 GS/s. Namely, the data in (a) are artificially created from the data in (b). (c) Three dimensional plot for parameters of pulse height versus $Q_{\rm fast}/Q_{\rm total}$ versus $Q_{\rm slow}/Q_{\rm total}$ for (b).

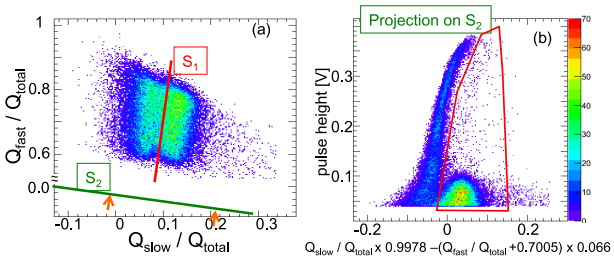

Fig. 7 Explanation of analysis procedure. (a) Pulse density plot on $Q_{\rm fast}/Q_{\rm total}$ versus $Q_{\rm slow}/Q_{\rm total}$ plane for the artificial data of 200 MS/s in Fig. 5. Surface S_1 and S_2 are also depicted. In this particular case, the surface S_1 and S_2 are expressed by $15\times Q_{\rm slow}/Q_{\rm total} - Q_{\rm fast}/Q_{\rm total} - 0.7005 = 0$, and $Q_{\rm slow}/Q_{\rm total} + 15\times Q_{\rm fast}/Q_{\rm total} = 0$, respectively. (b) Projected plot on surface S_2. The value of the horizontal axis is $(15\times Q_{\rm slow}/Q_{\rm total} - (Q_{\rm fast}/Q_{\rm total} + 0.7005))\times 0.0665$.

6) We determine the discrimination boundary using the projection shown in Fig. 7 (b).

By using the projection on S_2 in Fig. 7 (c), the contamination of γ-ray signals decreased by about 5% compared to using the conventional 2D projection on height $-Q_{\rm slow}/Q_{\rm total}$ in Fig. 3, for this particular data in the d-D neutron measurement. The easiness of availability of this complex procedure is a great advantage of the digital signal processing.

Another issue we have found relevant to the n-γ discrimination is the variation of the discrimination boundary to separate pulses due to neutrons and γ-rays. We supposed the boundary for the discrimination were static for a fixed detector set before experienced many cases of the digital signal analysis, and we expected we could discriminate signals for all plasma discharges once we determined the discrimination boundary. However, the detailed analysis revealed that this is not always true and discrimination boundary is not static. One case showing that the discrimination boundary are not static is a plasma discharges in which a counting rate increases up to $> 1\times 10^5$ cps. We

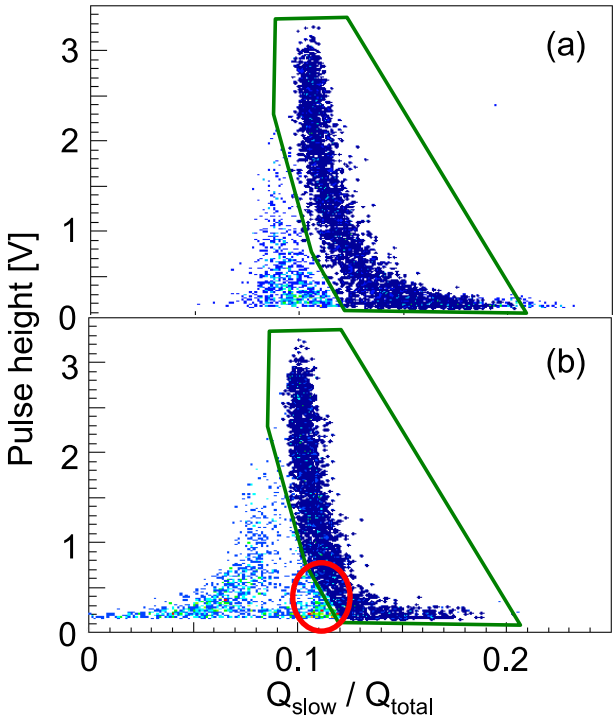

Fig. 8 Relation between pulses and a discrimination boundary indicated by solid lines in light green. The data was taken in the experiments for a 14 MeV neutron beam in FNS. (a) Discrimination boundary reasonably covered neutron pulses. (b) The boundary missed neutron pulses in a data set as indicated by a circle.

call this phenomenon a "pulse height variation" since the maximum pulse heights varies with counting rate. We describe this pulse height variation in the following section. Other cases were abrupt or sudden change of a discrimination boundary observed even in a series of similar discharges in JT-60U or measurements using a neutron beam in a neutron facility, FNS. The discrimination boundary became inappropriate suddenly in a particular data set, although the discrimination boundary became appropriate again in the subsequent data acquisition. One example is given in Fig. 8, which was observed in an experiment in

FNS. In this particular case, the area enclosed by a discrimination boundary reasonably covered data for neutron pulses, as shown in Fig. 8 (a), for other 40 sets of data in a series of acquisition, while the area missed neutron pulses in a particular data set as indicated in Fig. 8 (b). The time difference between each acquisition is less than 1 minute. Namely, the change is not a gradual change in a long time scale. In addition, the obvious difference in the experimental condition cannot be identified. So far, the reason of such change could not be traced yet sufficiently, but it looks due to the change in the condition in neutron detector and/or electronics. This phenomenon was observed both for several stilbene and NE-213 scintillators and also for three different types of PMTs (ELT 9266B type manufactured by Electron Tube Ltd., R1828-01 by Hamamatsu Photonics, H11934-100 by Hamamatsu Photonics), which were available to us.

Because of the variation of the discrimination boundary, we need to check the validity of the discrimination boundary for each data. Otherwise, there may be contamination of "neutron signal" with γ-ray pulses or vice versa. In other words, the conventional discrimination system using analog circuits could detect the contaminated "neutron signal" since the discrimination boundary is preset in the analog method or it is, in principle, impossible to carry out the post evaluation. The post evaluation of the discrimination boundary is an important advantage of the post process using the fast ADC.

4. Pulse Height Variation

In this section, the issue referred to as the "pulse height variation" is described in detail. The pulse height variation was observed when a count rate is higher than $\sim 1 \times 10^5$ counts/s. One example of this problem can be seen in Fig. 9 and Fig. 10. Figure 9 (a) depicts the temporal evolution of neutron emission rate measured by a fission chamber in JT-60U. The neutron emission rate increased rapidly up to about 8×10^{15} /s in this particular discharge. Figure 9 (b) is the temporal evolution of pulse height distribution and its time slices at three different periods are displayed in Fig. 9 (c). A maximum pulse height is dominated by γ-ray pulses in this particular case in Fig. 9 through Fig. 11. The maximum pulse height is varying in time as shown in Figs.9 (b) and (c), correlating with a neutron emission rate in Fig. 9 (a). Figure 10 plots the pulse height versus $Q_{\mathrm{slow}}/Q_{\mathrm{total}}$ against counting rate. Though arc shape, which is clearly seen in signals for γ-rays, can be observed in all cases, the curvature is larger in Fig. 10 (b) than Fig. 10 (a) or (c). This suggests the pulse is compressed in the vertical direction. Figure 11 shows the temporal evolution of d-D edge and the maximum pulse height. When we look into the details in Figs. 9 (a) and (c) and Fig. 11, we find that the signals with large pulse height, mainly by γ-rays, are affected while the pulses with low pulse height, mainly by d-D neutrons, are not so much.

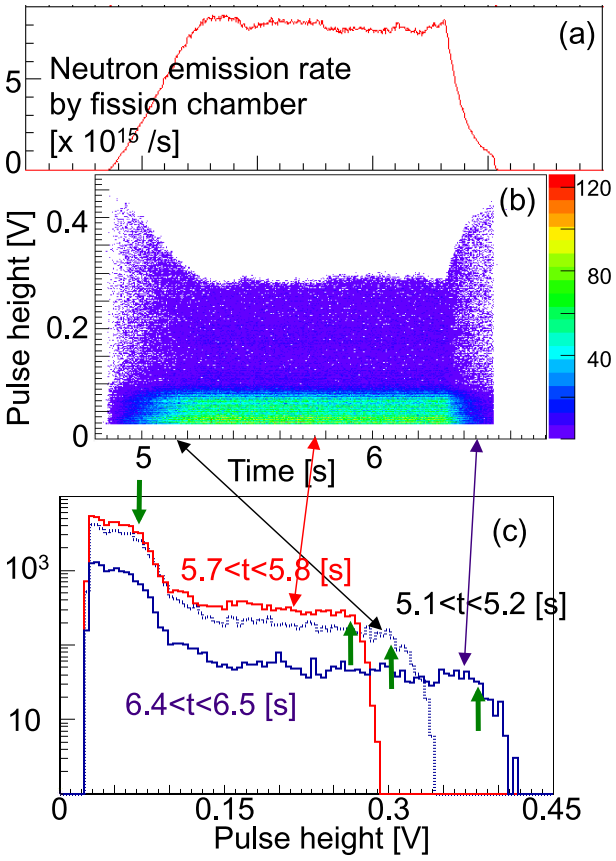

Fig. 9 Example case of "pulse height variation". (a) Volume integrated neutron emission rate measured by a fission chamber. (b) Temporal evolution of pulse height distribution. The maximum pulse height is changing in time. (c) Pulse height plots for three different time points indicated by arrows.

Namely, the gain of PMT decreases for large pulses selectively.

It is conjectured that the pulse height variation is caused when the average signal current is significant relative to the breeder current, in particular, at the last or second last stages of the dynode stages in a PMT [21]. Here, the breeder current includes electric charges from the capacitor equipped in this particular PMT. It is expected that unacceptable voltage drop, which leads to pulse height variation, easily occurs for pulses with high pulse height at the latter stage when the average signal current is large compared with breeder current, because even the capacitor cannot cover the electric charges required for the high pulse height.

An evidence for this conjecture can be seen in experimental results at FNS. Figure 12 shows the maximum pulse height dependence on the pulse count for the various value of the high voltage, HV, supplied to a PMT. The position of "edge" in the pulse height distribution represents the maximum pulse height. Here, the definition of the "edge" is the place where pulse count fall down rapidly in the pulse height distribution and its count is half

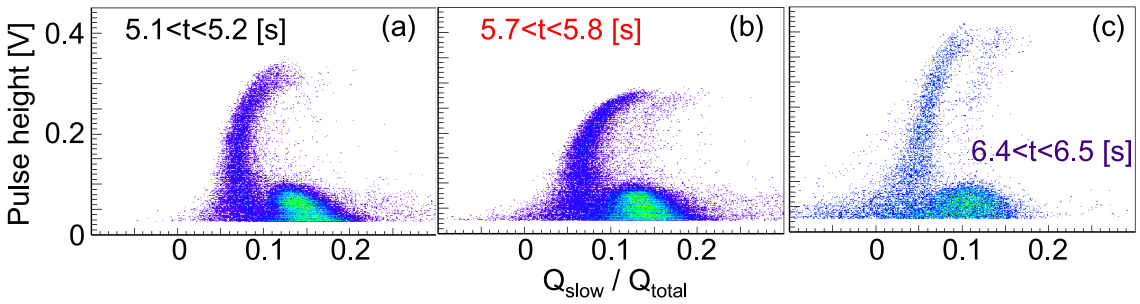

Fig. 10 Pulse density plots of pulse height versus Q_{slow}/Q_{total} for three different time points, which corresponds to plots in Fig. 9 (c).

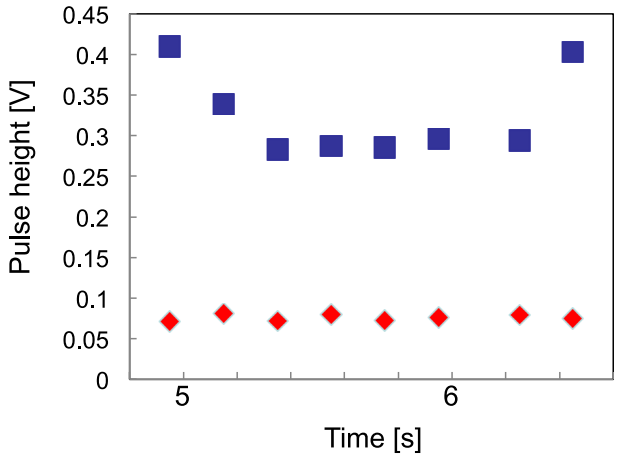

Fig. 11 Temporal evolution of d-D edge and maximum pulse height for the data in Fig. 9. The maximum pulse height is represented by the pulse height where the pulse count falls down to 10.

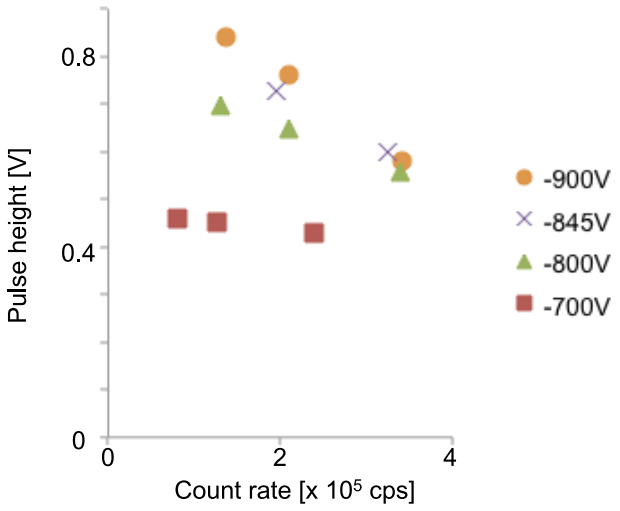

Fig. 12 "Edge" position in pulse height distribution versus pulse count rate for the pulses whose pulse height is above 0.05 V. Different markers indicate the different setting of high voltage of a PMT. This PMT was operated at −800 V in experiments on JT-60U.

of the count of the plateau region seen below the "edge". A strong dependence on the count rate indicates a serious pulse height variation. We observe higher HV setting induces a more serious pulse height variation. It is said that pulse height increases with HV exponentially whereas breeder current increases with HV linearly. Namely, the higher HV setting tends to cause the pulse height reduction. Thus, the result in Fig. 12 seems reasonable. The results indicate a PMT should be operated at an appropriate HV, which is somewhat lower than the conventional operation voltage of the PMT.

Based on the conjecture that the pulse height variation is caused by a lack of the breeder current, we reviewed hardware to avoid this problem on the breeder current, such as an active breeder using an FET circuit element [22]. We selected a booster method, in which dynode circuits at a few last dynode stages are supplied with electric current from the outer power supply with sufficient current capacity, because active electric circuits and a device to cool down the circuits are not required in a PMT.

The system can be simple and easy to handle if a power supply for the booster can be placed far outside the detector unit. It is necessary to confirm that the booster method works well even when the power supply is placed around 10 m away from a detector because the capacitor and the inductance in a long power line might prevent the PMT from responding to a pulse with a short time scale of a few ns. Therefore, we carried out experiment to test the booster method with a long power cable on FNS. In the experiments, we used a PMT, H11934-100 (Hamamatsu Photonics), and an NE-213 organic scintillator. The external power supply was connected to the circuits at the last three dynode-stages. The PMT was operated at the HV of −700 V. The plots of pulse height versus Q_{slow}/Q_{total} are depicted in Fig. 13. The 14 MeV d-T neutron beam was used to have a high pulse height. The upper plots (a) and (b) corresponds to the cases when the booster is switched off and the lower plots (c) and (d) corresponds to those when the booster is switched on. The left-hand-side plots (a) and (c) are for low neutron flux, and the right-hand-side ones (b) and (d) for high flux cases. We can see the system with the booster properly worked even with a long power cable in the high flux condition of $\sim 2 \times 10^5$ cps without

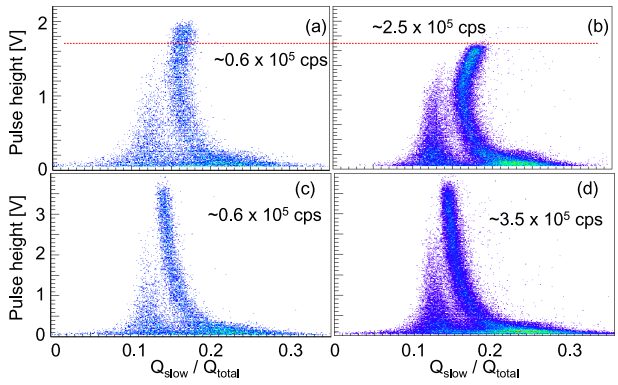

Fig. 13 Pulse height versus $Q_{\mathrm{slow}}/Q_{\mathrm{total}}$. (a) and (c) for low flux, (b) and (d) for high flux. The upper plots (a) and (b) are corresponds to the cases when the booster is switched off and the lower plots (c) and (d) are the cases when the booster is switched on. The pulse count for low flux is about 0.6×10^5 cps, while that for high flux is about $> 2.5 \times 10^5$ cps.

suffering from the pulse height variation.

5. Summary

A collimated neutron detection array system using a fast digitizer was operated on JT-60U. Since the entire waveform of pulses from a detector was recorded, this method revealed many detailed features in a neutron detection using an organic scintillator. In this paper, we described the features or issues that were revealed by using the fast digitizer for the first time, and the countermeasures to the issues.

To increase the quality of the n-γ discrimination method, it is important to find a time point, which separate the initial evolution of a pulse and its long-tail evolution. We looked into the detail of the pulse shape. We have confirmed the initial evolution could be explained by a model of a convolution of the response function of Gaussian in shape and the exponential decay curve. This model provides us a proper guide to determine the transition time from the initial evolution to the long tail evolution.

We investigated the better n-γ discrimination method. One of the advantages of the system using a fast digitizer is the availability of the multi-discrimination parameters. The distribution in multi-parameters suggested the conventional two-dimensional discrimination is not adequate to remove pulses from γ-rays due to noise and discreteness on digitizing waveforms. We have found the effect of the noise and the discreteness can be characterized by the parameters, $Q_{\mathrm{fast}}/Q_{\mathrm{total}}$ and $Q_{\mathrm{slow}}/Q_{\mathrm{total}}$. We have developed a new n-γ discrimination method. In the new method, we have introduced the analysis procedure to find an appropriate projection surface, on which we can define the discrimination boundary, in the three-dimensional space of the pulse height, $Q_{\mathrm{fast}}/Q_{\mathrm{total}}$ and $Q_{\mathrm{slow}}/Q_{\mathrm{total}}$. By using this projection, the contamination of γ-ray signals was decreased by about 5% in the d-D neutron measurement, compared to using the conventional 2D projection on height versus $Q_{\mathrm{slow}}/Q_{\mathrm{total}}$ for the particular data in Fig. 7.

We have also found that the discrimination boundary is not static and varying, so that the discrimination boundary for neutrons defined from a particular time in a particular discharge do not always applicable to the data in another discharge or time. This means that the conventional discrimination system using analog circuits could detect the contaminated "neutron signals" when the count rate is high, where the plasma performance is high, since the discrimination boundary is preset in advance or it is impossible to carry out the post evaluation. Unfortunately, the reliability of the system using an analog circuit could be reduced although the high-count rate is a preferable situation from the viewpoint of the statics of the pulse-counting measurement. Thus, because the reliability of the system relies on the validity of the discrimination boundary, the post evaluation of the discrimination boundary is an important advantage of the fast ADC. In the future work, we need to develop the method to determine the discrimination boundary automatically in order to establish the automatic discrimination system.

One of the causes to induce the variation of the discrimination boundary was a "pulse height variation" phenomenon, in which the maximum pulse height is reduced when a counting rate is high. We investigated the characteristic of the pulse height variation. We have found that pulses with a high pulse height are affected while those with a low pulse height are barely affected. We have also found the pulse height variation can be softened by operating a PMT at an appropriate HV, which is somewhat lower than the conventional operation voltage of the PMT in the experiments on FNS.

As a countermeasure against the pulse height variation, we picked up the booster method because the system could be simple. However, it was uncertain whether the booster method works properly with long power cables for the booster method since we need to use long power cables when we install the system on the experimental machine such as JT-60SA. We have carried out the experiments on this issue, using a 14 MeV d-T neutron beam on FNS. The results show the booster method successfully works in the high neutron flux condition of $\sim 2 \times 10^5$, avoiding the "pulse height variation", even with long cables of ~10 m.

We expect these results can contribute to a neutron camera system in ITER as well as in JT-60SA since a similar detection system using organic scintillators and PMTs are highly likely to be applied to them.

Acknowledgments

The authors would like to appreciate the JT-60 team and the FNS group for their contribution to the operation and the experiments at the JT-60U and FNS, respectively.

This work was supported by Grant-in-Aid for Scientific Research (B) (No. 19360420) and JSPS, Grant-in-Aid for Scientific Research (C) (No. 22560825).

[1] A.L. Roquemore, R.C. Chouniard, M. Diesso *et al.*, Rev. Sci. Instrum. **61**, 3163 (1990).
[2] J.M. Adams, O.N. Jarvis, G.J. Sadler *et al.*, Nucl. Instrum. Methods **329**, 277 (1993).
[3] O.N. Jarvis, J.M. Adams, F.B. Marcus and G.J. Sadler, Fusion Eng. Des. **34-35**, 59 (1997).
[4] M. Ishikawa, T. Nishitani, A. Morioka *et al.*, Rev. Sci. Instrum. **73**, 4237 (2002).
[5] W.W. Heidbrink *et al.*, Plasma Phys. Control. Fusion **46**, 1855 (2004).
[6] S.J. Zweben *et al.*, Nucl. Fusion **30**, 1551 (1990).
[7] D.S. Darrow *et al.*, Rev. Sci. Instrum. **66**, 476 (1995).
[8] S.S. Medley and A.L. Roquemore, Rev. Sci. Instrum. **69**, 2651 (1998).
[9] A. Klasilnikov *et al.*, J. Plasma Fusion Res. **75**, 967 (1999).
[10] M. Osakabe *et al.*, Rev. Sci. Instrum. **72**, 788 (2001).
[11] K. Shinohara, M. Takechi, M. Ishikawa *et al.*, Nucl. Fusion **42**, 942 (2002).
[12] M. Ishikawa, M. Takechi, K. Shinohara *et al.*, Nucl. Fusion **45**, 1474 (2005).
[13] M. Ishikawa, M. Takechi, K. Shinohara *et al.*, Nucl. Fusion **46**, S898 (2006).
[14] T. Suzuki *et al.*, Nucl. Fusion **48**, 045002 (2007).
[15] M. Ishikawa, T. Itoga, T. Okuji *et al.*, Rev. Sci. Instrum. **77**, 10E706 (2006).
[16] T. Itoga, M. Ishikawa, M. Baba *et al.*, Radiat. Prot. Dosimetry **126**, 380 (2007).
[17] K. Shinohara, T. Okuji, M. Ishikawa, M. Baba and T. Itoga, Rev. Sci. Instrum. **79**, 10E509 (2008).
[18] F.D. Brooks, Nucl. Instrum. Methods **162**, 477 (1979).
[19] K. Ishii, K. Shinohara, M. Ishikawa, T. Okuji, M. Baba, M. Isobe, S. Kitajima and M. Sasao, Plasma Fusion Res. **5**, S1043 (2010).
[20] K. Ishii, K. Shinohara, M. Ishikawa, M. Baba, M. Isobe, A. Okamoto, S. Kitajima and M. Sasao, Rev. Sci. Instrum. **81**, 10D334 (2010).
[21] *Photomultiplier tubes –Basics and Application* (Third Edition), Editted by T. Hakamata *et al.*, Hamamatsu Photonics K.K., (2005).
[22] M. Osakabe *et al.*, "Improvement of the neutron energy spectrometer, COTETRA (Counter Telescope with Thick Radiator)" in Proceedings of the international school of plasma physics "Piero Caldirola" workshop on Diagnostics for Experimental Fusion Reactor, September 4-12, 1997, Varena, Italy, ISBN 0-306-45835-7, printed in "Diagnostics for Experimental Thermonuclear Fusion Reactors 2 (No. 2)", Editted by P.E. Stott *et al.*, (Plenum Press, 1998), p.451.